20th Australasian Fluid Mechanics Conference
Perth, Australia
5-8 December 2016

Extending the Oscillatory Index to Discern Oscillatory Flow Modes

S. A. Gabriel[1], **Y. Ding**[1] **and Y. Feng**[2]

[1]Mathematical and Geospatial Sciences, School of Science
RMIT University, Melbourne, Victoria 3001, Australia

[2]Mineral Resources
CSIRO, Clayton South, Victoria 3169, Australia

Abstract

The Oscillatory Shear Index (OSI) metric is used extensively in cardiovascular flow studies to spatially quantify oscillatory flow behaviour. In its present form, the OSI is based on the wall shear stress, which restricts its scope to wall spaces and limits its relevance to the surrounding flow field. In the present study, this limitation is addressed with the introduction of the Oscillatory Flow Index (OFI), which is a unified extension of the OSI onto flow spaces. Collectively with the Oscillatory Kinetic Energy Index (OKEI), the two indices are used to differentiate between oscillatory "flow disturbances" by segregating direction-reversing modes of oscillation therein. Through assessment of a carotid bifurcation, the new indices are shown to correlate well with sites of oscillating flow and provide detail of their local oscillatory behaviour.

Introduction

Rhythmic contractions and relaxations of the heart generate regular pressure fluctuations that induce flow oscillations within the cardiovascular system [11]. Near the heart and particularly within arteries, flow oscillations significantly influence the net-periodic flow, such that it is said to be locally "disturbed" [9]. To describe the flow, its period-average is generally coupled with indices such as the Oscillatory Shear Index (OSI) [6, 7]. The OSI, which quantifies the oscillatory behaviour of the wall shear stress (WSS), is an extensively used index. Yet in its present form, it is by definition restricted to the walls. Herein, this limitation is addressed via extension of the index to the surrounding flow field, which directly influences its distribution.

A further limitation is expressed by the OSI's dominant receptivity to direction-reversing oscillatory modes, such that non direction-reversing modes are poorly recognised [9]. The distinction between these modes is of importance to the understanding of the influence that oscillatory "flow disturbances" [9] impart on endothelial cell behaviour [2] and mass transport [8]. As these are integral to atherogenesis, it is found that sites predisposed to atherosclerosis often coincide with low and oscillatory WSS [1, 7]. This correlation is imprecise, particularly with respect to the role of flow oscillations, yet it is one of the prevailing theories regarding flow-mediated atherogenesis [10]. In the objective of refining these correlations, the OSI is further developed to differentiate between oscillatory modes, so that the role of flow oscillations may be distilled.

Methodology

Blood is a heterogeneous fluid, comprising a suspension of particulates such as erythrocytes, thrombocytes and leukocytes. Whilst all relevant measurements are generally made at the macroscale, it is at the microscale level of the particulates where many significant interactions are expressed [11]. The explicit resolution of both scales in computational models of medium-large sized blood vessels is for the present prohibitive. To bypass this limitation, a continuum hypothesis is generally assumed for the blood medium, whereby the macroscale flow is resolved and the microscale modelled. In doing so, macroscale level properties such as rheology may be satisfactorily described via constitutive models [11].

Governing Equations

Blood flow is therefore described by the incompressible mass and momentum (Navier–Stokes) conservation equations, which are respectively defined in conservative-form, by:

$$\partial_i u_i = 0 \tag{1}$$

$$\rho\partial_t u_i + \partial_j\left(\rho u_i u_j - \tau_{ij} + p\delta_{ij}\right) = 0 \tag{2}$$

where u_i is the blood's velocity-vector field and ρ its density, p is its scalar pressure field, and δ_{ij} is the Kronecker delta. The stress tensor $\tau_{ij} = 2\mu D_{ij}$ is defined proportional to the strain-rate (rate of deformation) tensor $D_{ij} = \frac{1}{2}\left(\partial_i u_j + \partial_j u_i\right)$, where viscosity $\mu(\dot\gamma)$ is a function of the strain-rate tensor magnitude $\dot\gamma = \sqrt{2D_{ij}D_{ij}}$. For the present formulation, blood density is a constant $\rho = 1050\ \left[\mathrm{kg/m^3}\right]$, and viscosity is strain-rate dependant (non-Newtonian), modelled by the Carreau formulation:

$$\mu(\dot\gamma) = \mu_\infty + (\mu_0 - \mu_\infty)\left[1 + (\lambda\dot\gamma)^2\right]^{(n-1)/2} \tag{3}$$

where the parameters are defined $\lambda = 3.313\ [\mathrm{s}]$, $n = 0.3568$, and the zero and infinite strain limit viscosities are respectively defined $\mu_0 = 0.056\ [\mathrm{kg/m/s}]$ and $\mu_\infty = 0.00345\ [\mathrm{kg/m/s}]$ [3].

Geometry

In geometrically regular flow spaces, such as within uniformly tubular vessel segments, blood flow generally remains "stable". However, at sites of geometric irregularities, transient flow disturbances may emerge [4]. Such conditions are found at the geometric and topologic changes inherent to vascular bifurcations, which lend them to host flow structures that induce flow disturbances, such as recirculating flow zones [4]. Therefore, to demonstrate the capability of the introduced indices in measuring oscillatory flow disturbances, the subject geometry of the present study is an arterial bifurcation, namely of a human carotid*. A schematic diagram of the geometry is presented in figure 1, where Ω_f denotes the volumetric flow space of the artery, which is bounded by the wall Γ_w and inflow/outflow boundaries of the common (CCA) Γ_C, internal (ICA) Γ_I and external (ECA) Γ_E carotid arteries. For the present study, the arterial wall is non-compliant, therefore all field-variables are processed within a fixed Eulerian reference frame.

Note on notation: The subscripts i, j are reserved for index notation of Cartesian tensors; all other subscripts are for designating variables, and should not be interpreted as tensor indices. Repeated indices in a term imply Einstein summation notation. For the generic vector φ_i, the element-wise absolute is designated by the vector $|\varphi_i|$ and the Euclidean magnitude (2-norm) by the scalar $\|\varphi_i\| = \sqrt{\varphi_i\varphi_i}$.

*Source: http://grabcad.com/library/carotid-bifurcation

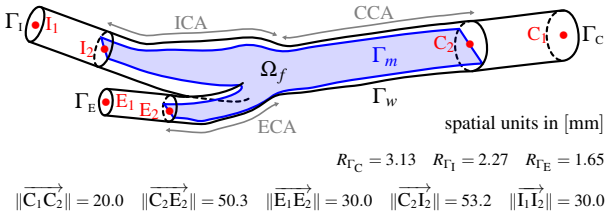

Figure 1: Schematic of the carotid artery geometry, with mid-surface Γ_m and inflow/outflow extensions. Dimensions are given by the average radius R_Γ of inflow/outflow boundaries and distance between centroids of successive cross-sections. Flow extension lengths are not to scale.

Boundary Conditions

Uniform outflow conditions of the form $u_i n_i = Q/\int \mathrm{d}\Gamma$ are assigned to boundaries Γ_I and Γ_E, where $n_i = \partial_i \Gamma$ is the unit normal to the respective boundaries, and the flow-rate Q is transient and defined at its respective boundary according to the periodic forms in figure 2. In the present formulation, the flow is solely driven by a pressure gradient. Therefore, to gauge-fix the pressure field, an arbitrarily chosen Dirichlet boundary condition $p = 0$ is applied at boundary Γ_C. For the wall boundary Γ_w, a no-slip wall condition is assigned, such that $u_i = 0$.

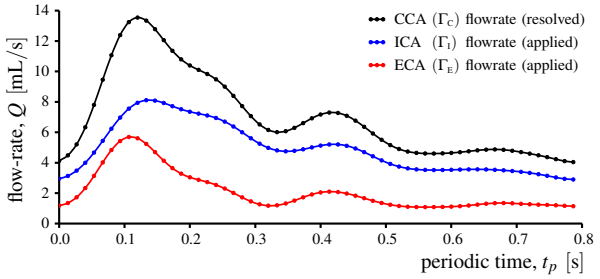

Figure 2: Periodic flow-rate waveforms applied as boundary conditions at the ECA and ICA, with the equivalent waveform at the CCA (not applied); adapted from [5].

As the inflow and outflow boundary conditions are defined uniformly on their respective boundaries, they may not locally resemble an accurate flow field. Therefore, flow extensions are implemented between the respective boundaries and the carotid artery geometry (see figure 1), so that flow within the latter is sufficiently developed and independent of the boundary condition limitations. At the CCA's inflow boundary, the equivalent flow profile resolves to a period-averaged Reynolds number of $Re|_{\Gamma_\mathrm{C}} = 427$. Its corresponding velocity magnitude $u_0 = \int \overline{u}_i n_i \,\mathrm{d}\Gamma_\mathrm{C} / \int \mathrm{d}\Gamma_\mathrm{C}$ and Poiseuille WSS $\tau_{w0} = 4\mu_\infty u_0 / R_{\Gamma_\mathrm{C}}$ will be used as reference values for the flow field.

Oscillatory Flow Decomposition

To characterise the oscillatory nature of the flow, an arbitrary scalar field-variable φ that is transported within oscillatory flow of period-length T_p is considered. Following Reynolds periodic-decomposition, the period-average $\overline{\varphi}$ and time-dependent perturbation φ' components may be realised:

$$\begin{aligned} \varphi(t) &= \overline{\varphi} + \varphi'(t) \\ \text{where} \quad \overline{\varphi} &= \frac{1}{T}\int_T \varphi(t)\,\mathrm{d}t, \quad t \in T \end{aligned} \tag{4}$$

The integration length is defined $T = kT_p$, where $k \geq 1$ is an integer multiplier. For laminar flow conditions, the integration may be made over a single period of oscillation ($k = 1$), since the flow field is periodic at all relevant length scales. However, in turbulent flow conditions, a sufficiently large number of periods ($k >> 1$) would be required for $\overline{\varphi}$ to become temporally invariant. This decomposition is illustrated in the phase portrait of figure 3, which expresses the φ_i oscillation as a closed loop about the period-average $\overline{\varphi}_i$. Should the loop be non-singular (i. e. not a point) and centred about $\overline{\varphi}_i = 0$, it is referred as a pure oscillation of a direction-reversing (DR) mode. If the loop does not cross $\varphi_i = 0$ axes, it is referred as a non direction-reversing (NDR) mode. Combinations of these behaviours would be regarded as mixed DR/NDR modes.

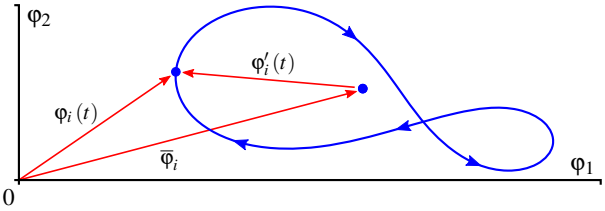

Figure 3: Oscillatory phase portrait of φ_i, at an arbitrary point in a 2-dimensional flow (same principle in 3-dimensions).

Oscillatory Indices

To differentiate between the two modes of oscillation, the Oscillatory Index (OI) is used. This measure is a generalisation of the Oscillatory Shear Index (OSI) [6, 7], and is used to quantify the oscillatory nature of the flow. Based on the original form of the OSI [6], the OI of a generic field-variable φ_i is defined:

$$\mathrm{OI}_0\{\varphi_i\} = \frac{1}{2}\left(1 - \frac{\left\|\frac{1}{T}\int_T \varphi_i \,\mathrm{d}t\right\|}{\frac{1}{T}\int_T \|\varphi_i\| \,\mathrm{d}t}\right) \tag{5}$$

The OSI may be defined as a special case of the OI, such that $\mathrm{OSI} \equiv \mathrm{OI}\{\tau_{wi}\}$, where $\tau_{wi} = \Theta_i - \left(\Theta_j n_j\right) n_i$ is the WSS vector; defined as the wall-tangential decomposition of the traction stress vector $\Theta_i = \tau_{ij} n_j$, where n_i in this context is the unit normal vector to the wall boundary Γ_w. In the same manner, the Oscillatory Flow Velocity Index (OFVI) may be defined to characterise the flow field u_i, such that $\mathrm{OFVI} \equiv \mathrm{OI}\{u_i\}$.

The OI measures the oscillatory deviation that φ_i experiences relative to its period-average. In its original form, it was not designed to differentiate between the modes of oscillation. Therefore, in the present analysis, a subtle modification is made to the OI, in favour of exclusively measuring DR oscillations:

$$\mathrm{OI}_1\{\varphi\} = \frac{1}{2}\left(1 - \frac{\left\|\frac{1}{T}\int_T \varphi_i \,\mathrm{d}t\right\|}{\left\|\frac{1}{T}\int_T |\varphi_i| \,\mathrm{d}t\right\|}\right) \tag{6}$$

In both the original and modified form, the OI is defined to take its minimum limiting value (0) at a non-oscillatory flow, and its maximum limiting value (0.5) at a pure DR oscillatory mode. The modified form of the OI is also designed to filter out NDR oscillatory modes, such that they return a zero value; whereas in the original form, NDR modes would return near-zero values, though not exactly zero. This distinction is necessary, as it will be used to differentiate between the two modes of oscillation.

Another useful measure of flow oscillations is their energy, which is invariant to the mode of oscillation. By applying Reynolds periodic-decomposition (equation 4) to an oscillatory flow field u_i, its period-average $\overline{u}_i$ and time-dependent perturbation u_i' may be obtained. It follows that the flow's period-averaged kinetic energy (per unit mass), may be decomposed into a dependence on the period-averaged flow $\overline{\kappa}_{\overline{u}} = \frac{1}{2}\overline{u}_i\overline{u}_i$ and its perturbations $\overline{\kappa}_{u'} = \frac{1}{2}\overline{u_i' u_i'}$ respectively. Therefore, to quantify the relevance of oscillatory perturbations within a periodic

flow, the quotient of their respective energies is used; this is represented by the Oscillatory Kinetic Energy Index:

$$\mathrm{OKEI} \;=\; \overline{\kappa}_{u'} \big/ \left(\overline{\kappa}_{\overline{u}} + \overline{\kappa}_{u'}\right) \tag{7}$$

Unification of Oscillatory Indices on Flow and Wall Spaces

By definition, the OKEI and OFVI are restricted to flow spaces, and the OSI to walls. This presents an inconvenience, as both flow and wall spaces are assessed in haemodynamic analyses. To overcome this limitation, the behaviour of these indices at the flow–wall limit is considered. It is noted, that the WSS at a point on a wall is proportional to the wall-tangential flow velocity u_i^t at an infinitesimal distance ε_w, normal to the wall surface:

$$\tau_{wi} \;\propto\; \lim_{\varepsilon_w \to 0} \frac{u_i^t\big|_{\varepsilon_w}}{\varepsilon_w} \tag{8}$$

By taking advantage of the indices being expressed as one-to-one quotients of their respective field-variables, a unification may be achieved. It follows via equation 8, that the OSI may be related to the OFVI in the limit near the wall by the relation:

$$\begin{aligned}
\lim_{\varepsilon_w \to 0} \mathrm{OI}_1\left\{u_i^t\right\}\big|_{\varepsilon_w} \;&=\; \lim_{\varepsilon_w \to 0} \frac{1}{2}\left(1 - \frac{\left\| \frac{1}{T}\int_T u_i^t\big|_{\varepsilon_w}\,\mathrm{d}t \right\|}{\left\| \frac{1}{T}\int_T \left| u_i^t\big|_{\varepsilon_w} \right| \mathrm{d}t \right\|}\right) \\
&=\; \lim_{\varepsilon_w \to 0} \frac{1}{2}\left(1 - \frac{\left\| \frac{1}{T}\int_T \frac{u_i^t|_{\varepsilon_w}}{\varepsilon_w}\,\mathrm{d}t \right\|}{\left\| \frac{1}{T}\int_T \left| \frac{u_i^t|_{\varepsilon_w}}{\varepsilon_w} \right| \mathrm{d}t \right\|}\right) \\
&=\; \frac{1}{2}\left(1 - \frac{\left\| \frac{1}{T}\int_T \tau_{wi}\,\mathrm{d}t \right\|}{\left\| \frac{1}{T}\int_T |\tau_{wi}|\,\mathrm{d}t \right\|}\right) \\
&=\; \mathrm{OI}_1\left\{\tau_{wi}\right\}
\end{aligned}$$

This relation is only applicable to the wall-tangential component of the near-wall flow, and also holds for OI_0. As the OFVI tends to the OSI in the near-wall limit, it follows that a unified index, the Oscillatory Flow Index (OFI) may be constructed:

$$\mathrm{OFI} \;=\; \begin{cases} \mathrm{OI}\{u_i\} & \text{on} \quad \Omega_f \cup \partial\Omega_f \setminus \Gamma_w \\ \mathrm{OI}\{\tau_{wi}\} & \text{on} \quad \Gamma_w \end{cases} \tag{9}$$

Following the same generalisation, the OKEI is also extended:

$$\mathrm{OKEI} \;=\; \begin{cases} \dfrac{\overline{u_i' u_i'}}{\overline{u}_i \overline{u}_i + \overline{u_i' u_i'}} & \text{on} \quad \Omega_f \cup \partial\Omega_f \setminus \Gamma_w \\ \dfrac{\overline{\tau_{w_i}' \tau_{w_i}'}}{\overline{\tau_{w_i}}\,\overline{\tau_{w_i}} + \overline{\tau_{w_i}' \tau_{w_i}'}} & \text{on} \quad \Gamma_w \end{cases} \tag{10}$$

Segregating and Measuring DR / NDR Oscillations

The OKEI is a measure of flow oscillations and is indiscriminate of their mode, whereas the OI_1 has been constructed to measure DR oscillations exclusively. It follows, that the OI_1 may be used to filter out oscillatory modes within the OKEI. This filtering is constructed for the DR and NDR modes respectively:

$$\mathrm{OKEI}_{\mathrm{DR}} \;=\; \mathrm{OKEI} \times \mathrm{OFI}_1 \tag{11}$$

$$\mathrm{OKEI}_{\mathrm{NDR}} \;=\; \mathrm{OKEI} \times \left(1 - 2 \times \mathrm{OFI}_1\right) \tag{12}$$

The range for these indices is the same as that of the OKEI. Where the lower and upper limits $0 \leq \mathrm{OKEI} \leq 1$ respectively indicate a non-oscillatory and purely oscillatory flow; a critical balance between the kinetic energies of the oscillatory and mean-flow is met at $\mathrm{OKEI} = 0.5$.

Results and Discussion

The system of equations was implemented into the cell-centred finite-volume solver ANSYS Fluent v16.2, and solved for the carotid geometry of figure 1, which was discretised with a hybrid polyhedral/hexahedral mesh; following successive refinement for mesh independence of the flow field velocity, a final converged mesh of 1.73×10^6 elements was used for this study. The SIMPLE algorithm was used for pressure-velocity coupling, with pressure discretisation using the 'standard' scheme (neighbour-cell interpolation using momentum-equation coefficient weighting). For momentum (flow) variables, a second-order upwind discretisation was used, and for field-variable gradients, a least-squares cell-based interpolation. Temporal discretisation was made with an implicit first-order forward-differencing scheme. Computations were made with double-precision on a 64-bit serial machine. Following successive computed periods P, the fifth period was deemed sufficiently purged from association with (zero) initial conditions, and used to process data on the sixth period; the periodic flow residual criterion $R_{\overline{u}} < 10^{-5}$ was used to determine this cut-off, where:

$$R_{\overline{u}}\left(m_p\right) \;=\; \left| \left[\int_{\Omega_f} \|\overline{u}_i\|\,\mathrm{d}\Omega \Big/ u_0 \int_{\Omega_f} \mathrm{d}\Omega \right]_{P=m_p}^{P=m_p+1} \right| \tag{13}$$

Following numeric convergence, results are post-processed on mid-surface Γ_m, cut-planes and the arterial wall Γ_w, for flow and wall variables respectively. The flow and WSS field-variables are displayed in figure 4, and oscillatory flow indices in figure 5. To demonstrate the significance of the derived indices, they are related to flow structures observed within the carotid. Starting at the uniformly tubular CCA, the period-averaged flow field of figure 4 reveals a stable flow and WSS distribution that maintains unidirectionality. This is registered by the oscillatory flow indices (figure 5), which describe a period-average dominated flow ($\mathrm{OKEI} < 0.5$) with a distribution of weak oscillatory NDR modes. Near the wall, where viscous terms dominate, the oscillatory influence is greatest and may act to disturb the near-wall flow and hence the WSS (figure 4), which is an important parameter in haemodynamics. However, being of weak NDR modes, the oscillatory influence may not be significant.

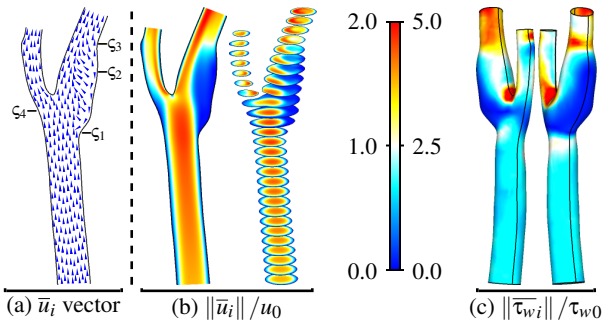

Figure 4: Distribution of (a) normalised velocity vectors, and dimensionless (b) velocity magnitude and (c) wall shear stress.

As the flow approaches the carotid bifurcation, disturbances emerge in response to the topologic and geometric changes encountered therein. At the entrance of the ICA, the flow separates at location ς_1 and forms a recirculation zone up to ς_2, where it reattaches (refer to the velocity vector plot in figure 4). Within an oscillatory period, both separating and reattaching flow experience corresponding oscillations. Physically interpreted, this implies that the size of the recirculation zone oscillates in response to the globally oscillating flow field. This is reflected by the presence of dominant DR modes at both reattaching and separating flow sites (figure 5). However, relative to the reattaching

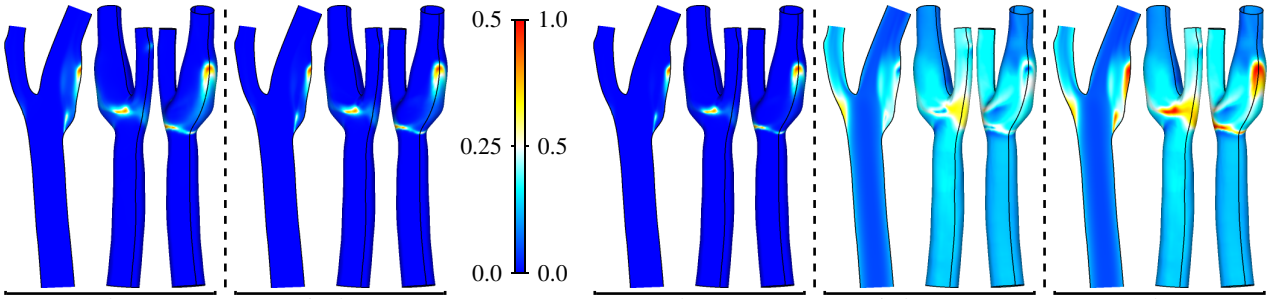

(a) OFI_0 (b) OFI_1 (c) $OKEI_{DR}$ (d) $OKEI_{NDR}$ (e) OKEI

Figure 5: Distribution of oscillatory flow indices (on mid-surface Γ_m and the arterial wall Γ_w; front and back view). Note that both OFI_1 and $OKEI_{DR}$ distributions resemble that of OFI_0; though OFI_1 is an exclusive DR mode measure, and $OKEI_{DR}$ is OKEI-weighted.

flow, the separating flow has a stronger geometric dependence within the non-compliant artery, and is therefore restricted from oscillating to a greater extent. Correspondingly, $OKEI_{DR}$ of the separating flow is lower in magnitude and spatially smaller than that of the reattaching flow, which has greater oscillatory space.

Though DR oscillatory modes influence the bounds of the recirculation zone, NDR modes dominate within the structure and remain confined to it. This is indicative of an aggregate of oscillatory disturbances within the recirculation zone, which due to the barrier that the recirculating flow structure forms, are not advected away by the surrounding flow field. Downstream of the recirculation zone, the flow quickly recovers up to ς_3, where it returns to a relatively unidirectional state up to the ICA outlet, and OKEI tends to zero. Conversely, the period averaged flow at the entrance of the ECA (location ς_4) also forms a low velocity-magnitude zone, which remains attached to the wall. The structure is NDR mode dominated, and unlike the ICA recirculation zone, it does not form an enclosing environment. The NDR mode oscillations are therefore free to propagate downstream into the ECA and disturb the surrounding flow field.

Conclusion

This study presents the Oscillatory Flow Index (OFI) to quantify "disturbed" oscillatory flow. The index is a unified extension of the widely used OSI onto flow spaces, such that the latter's distribution on wall spaces may be seamlessly related to oscillatory flow field behaviour. It is demonstrated that oscillatory flows may be categorized into a spectrum ranging from direction-reversing (DR) to non direction-reversing (NDR) modes, which the introduced Oscillatory Kinetic Energy Index (OKEI) collectively measures and the OFI may be used to segregate. These indices are studied on an anatomically realistic carotid, revealing a high predisposition of the site of bifurcation to flow disturbances that arise from the geometric variations encountered therein. The derived indices also reveal that DR modes are most prominent at sites of separating and reattaching flow, and generally remain confined to their sources. Whereas NDR modes are spatially spread and propagate from their source, which may be of either DR or NDR modes. These outcomes indicate that oscillatory flow behaviour varies and can be generalised by segregating its respective modes. It is therefore proposed, that correlations to flow-mediated physiologic responses, such as atherogenesis, may be refined by segregating oscillatory flow modes.

Acknowledgements

This research was supported by an Australian Postgraduate Award and a grant from the CSIRO, through the ATN Industry Doctoral Training Centre. The contributions of Dr John Gear in preparation of the research are also acknowledged.

References

[1] Cecchi, E. et al., Role of hemodynamic shear stress in cardiovascular disease, *Atherosclerosis*, **214**, 2011, 249–56.

[2] Chatzizisis, Y. S. et al., Role of endothelial shear stress in the natural history of coronary atherosclerosis and vascular remodeling: molecular, cellular, and vascular behavior, *Journal of the American College of Cardiology*, **49**, 2007, 2379–93.

[3] Cho, Y. I. and Kensey, K. R., Effects of the non-Newtonian viscosity of blood on flows in a diseased arterial vessel. Part 1: Steady flows, *Biorheology*, **28**, 1991, 241–62.

[4] Dhawan, S. S. et al., Shear stress and plaque development, *Expert Review of Cardiovascular Therapy*, **8**, 2010, 545–56.

[5] Dong, J., Wong, K. K. L. and Tu, J., Hemodynamics analysis of patient-specific carotid bifurcation: a CFD model of downstream peripheral vascular impedance, *International journal for numerical methods in biomedical engineering*, **29**, 2013, 476–91.

[6] He, X. and Ku, D. N., Pulsatile flow in the human left coronary artery bifurcation: average conditions, *Journal of biomechanical engineering*, **118**, 1996, 74–82.

[7] Ku, D. N., Giddens, D. P., Zarins, C. K. and Glagov, S., Pulsatile flow and atherosclerosis in the human carotid bifurcation. Positive correlation between plaque location and low oscillating shear stress, *Arteriosclerosis, Thrombosis, and Vascular Biology*, **5**, 1985, 293–302.

[8] Liu, X., Fan, Y., Deng, X. and Zhan, F., Effect of non-Newtonian and pulsatile blood flow on mass transport in the human aorta, *Journal of biomechanics*, **44**, 2011, 1123–31.

[9] Peiffer, V., Sherwin, S. J. and Weinberg, P. D., Computation in the rabbit aorta of a new metric - the transverse wall shear stress - to quantify the multidirectional character of disturbed blood flow, *Journal of biomechanics*, **46**, 2013, 2651–8.

[10] Peiffer, V., Sherwin, S. J. and Weinberg, P. D., Does low and oscillatory wall shear stress correlate spatially with early atherosclerosis? A systematic review, *Cardiovascular research*, **99**, 2013, 242–50.

[11] Thiriet, M., *Biology and Mechanics of Blood Flows. Part II: Mechanics and Medical Aspects*, Springer New York, New York, NY, 2008.